MODAL ANALYSIS USING TIME-AVERAGE PANORAMIC HOLO-INTERFEROMETRY[1]

by

Jeffrey L. Lindner and John A. Gilbert[2]

Abstract

Holographic analysis of complex structures is often difficult. One of the major problems is that the limited field of view available with current holographic inspection systems restricts the extent to which a full assessment of the structure may be made. In many cases, it becomes necessary to superimpose data extracted from spot views to characterize the modal response.

This paper describes a new approach to modal analysis in which time-average holograms are recorded through a panoramic system. When inserted into a cylindrical structure, the system allows a relatively large portion of the surroundings to be illuminated and observed. The approach is applied to study the modal response of an aluminum ring. Quantitative results agree well with those obtained using standard impact hammer testing; qualitative comparisons are made between panoramic holo-interferograms recorded on the inner wall and those recorded on the outer surface using standard time-average holographic recording techniques. The main advantage of time-average panoramic holo-interferometry over conventional holo-interferometric recording is that displacement is recorded with nearly constant sensitivity over the entire field of view, making it simpler to qualitatively analyze the modal response.

---

[1] This work was presented at the Eleventh International Modal Analysis Conference, Kissimmee, Florida, February 1-4, 1993.

[2] Jeffrey L. Lindner is a test engineer in the Structures and Dynamics Laboratory of NASA's George C. Marshall Space Flight Center, MSFC, AL 35812; John A. Gilbert is a professor of mechanical engineering at the University of Alabama in Huntsville, Huntsville, AL 35899.

Nomenclature

$\hat{\mathbf{e}}_i$	unit vector
$\mathbf{d}$	displacement vector
$\mathbf{g}$	sensitivity vector
r,θ,z	cylindrical coordinates in object space
r',θ'	polar coordinates in image plane
x,y,z	Cartesian coordinates in object space
x',y'	Cartesian coordinates in image plane
w	scaler displacement component
I	intensity
N_i	roots of the zero order Bessel function
J_o	zero order Bessel function
RR	repeated root
S	source point
O	observation point
P	model point
PAL	panoramic annular lens
λ	wavelength

Introduction

At NASA's Marshall Space Flight Center modal testing is primarily used as a tool for tuning finite element models. In recent years, modal characterization requirements have broadened, stimulating the development of new advanced modal parameter acquisition techniques such as time-average holo-interferometry.

The time-average holographic recording technique, developed by Stetson and Powell,[1] can be used to reveal contours of constant amplitude on the surface of a vibrating object. In this technique, a holo-interferogram is produced by generating a hologram and exposing the recording medium for a period of time during which the test object executes many cycles of steady vibration. In this case, the intensity of the reconstructed image is

$$I \propto J_o^2 \left[\frac{2\pi}{\lambda} (g \cdot d)\right] \quad (1)$$

where λ is the wavelength of the coherent light used to record and reconstruct the hologram, **d** is the displacement vector of the surface point under consideration, and J_o is the zero order Bessel function. The sensitivity vector **g** is defined by $(\hat{\mathbf{e}}_2 - \hat{\mathbf{e}}_1)$ where $\hat{\mathbf{e}}_1$ and $\hat{\mathbf{e}}_2$ are unit vectors in the directions of illumination and observation, respectively.

When the displacement is zero, the reconstructed image is the brightest; consequently, regions having no motion, or nodes in the vibratory pattern, exhibit the greatest intensity. Dark fringes occur at the roots (zeros) of J_o^2; the particular root on the interferogram may be determined by counting from the nearest stationary point on the object, marked by the very bright fringe corresponding to the nodal location. The roots of J_o are tabulated and their values may be used together with the known values of the sensitivity vector to determine the amplitude of the object motion in the direction of the sensitivity vector.

If a hologram is recorded of the object while it is vibrating in only one of its vibration modes, then a photograph of the reconstruction from that hologram will display the vibration mode in a simple topographical map of fringe contours. For example, with normal illumination and observation,

$$N_i = \frac{4\pi w}{\lambda} \quad (2)$$

where w is the displacement component along the line of sight and N_i are the roots of the Bessel function. This presumes that the sensitivity vector is essentially constant across the surface of the object, and that the vibratory motion is unidirectional.

In some cases, vibration analysis may require more than one holographic perspective per

mode. For example, when studying a test article with an irregular or a complex shape, it may be impossible to illuminate the entire area of interest from a single position or view the area from a single hologram. In these cases, it becomes necessary to vary the orientation of the test article or to modify the conventional holographic recording setup to obtain the required information. This procedure substantially increases data acquisition time and produces data that is often difficult to interpret, since information from several holographic recordings must be combined to accurately describe a given mode shape.

The situation becomes even more difficult when measurements must be made within rocket engine machinery such as bearing cages, pressures vessels and turbine inlet bellows. Even though significant progress has been made in the development of holographic tools and techniques, only a small fraction of the work performed in the area of holo-interferometry deals with making measurements within such cavities. In general, most attempts to record holograms over extended areas in confined spaces have met with limited success, mainly because current holographic systems provide only spot views within the region of interest. This problem can be eased somewhat by employing a panoramic imaging system.

The first attempt to patent a system for panoramic imaging was made by Mangin in 1878,[2] and since that time numerous other devices have been patented.[3] Most of these devices depended on a scanning system or on a complex set of lenses. The inherent design features made it difficult to utilize these panoramic systems for making measurements. However, in 1984, Greguss invented a simple lens known as a panoramic annular lens capable of giving a full 360° surround of the area around the lens. The following sections provide more details about this lens and describe a new approach to modal analysis in which time-average holograms are recorded through a panoramic system.

The Panoramic Annular Lens

The *Panoramic Annular Lens* (PAL) consists of a single piece of glass with spherical surfaces that produces a flat annular image of the entire 360° surround of the optical axis of the lens. As illustrated in Figure 1, light is reflected and refracted within the lens to form a virtual image. This image must be conveyed to an image capturing device using a transfer lens. This is illustrated in Figure 2 which shows the schematic of a commercially available PAL imaging system. The system includes a 38 mm diameter PAL mounted with an f/1.4, 25 mm focal length transfer lens. The field of view extends from approximately -20° below the lens to 25° above the lens; a "C" mount is included so that the system can be attached to a standard video camera. The PAL can also be used with a compound lens system or, by itself, to illuminate the wall of a cavity. The angular resolution varies as the viewing angle changes from below to above the lens but is generally about 5 milliradians. The effective acceptance angle of the PAL is quite small, and the PAL is a rather slow lens, compared to traditional lenses. The most outstanding attributes of the PAL, on the other hand, are that there are no moving parts, the area surrounding the lens can be viewed simultaneously, and the depth of focus extends from its surface to infinity. These attributes have made it possible to measure displacements within cavities using double-exposure and real-time holographic recording techniques.[4-6] This paper introduces time-average panoramic holo-interferometry.

Time-Average Panoramic Holo-Interferometry

Time average panoramic holo-interferometry relies on the standard time-average holographic method and utilizes two PALs; one to illuminate and the other to view the inner wall of a cavity. The PAL produces an annular image; the Cartesian (x',y') and polar (r',θ') coordinate systems used to define this image are shown superimposed on Figure 1. Figure 3, on the other

hand, defines the Cartesian (x,y,z) and cylindrical (r,θ,z) coordinate systems used to describe object space.

Referring to Figure 3, it is assumed that two opposing collinear PALs are aligned with their optical axes along the z-direction. Coherent light is projected by one PAL from the source point S to a point P located on the wall of a cavity, depicted in the figure as a ring. The image of P is observed by the second PAL at point O. For analysis purposes, unit vectors $\hat{\mathbf{e}}_1$ and $\hat{\mathbf{e}}_2$ are shown in the direction of illumination and in the direction of observation, respectively. The sensitivity vector, **g**, described in Equation (1), lies along the angle bisector of $\hat{\mathbf{e}}_1$ and $\hat{\mathbf{e}}_2$.

Figure 4 illustrates how the sensitivity vector is modulated when two opposing collinear PALs are used to record a holo-interferogram. In the center of the illuminated band, **g** is perpendicular to the optical axis of the system and only radial displacements are measured. Toward the edges of the band, however, **g** becomes inclined. Assuming that the displacement is purely radial, an error is introduced which depends on the spacing between the lenses and the width of the band. For a more complex situation, the displacement component parallel to the optical axis influences the holographic fringe pattern in areas where the sensitivity vector is inclined; whereas, the circumferential displacement component does not effect the fringe pattern.

Experimental

A data base defining the modal parameters of an aluminum ring measuring 10.16 cm (4.00") diameter, 2.13 cm (0.84") length and 1.27 mm (0.05") wall thickness was acquired to evaluate holographic test results. This was accomplished with impact hammer modal testing techniques employing an HP 5423A Structural Dynamics Analyzer. In these tests, the ring was supported by three elastic cords producing a free-free boundary condition. A small Piezotronics, Inc. model GK291B80 calibrated hammer, configured as a pendulum, was used to excite the ring.

By the theory of reciprocity, the impact hammer was roved from point to point while response measurements were acquired with a Piezotronics, Inc. model 309A accelerometer oriented radially and bonded to the ring with super-glue. The additional mass of the accelerometer effected the modal content of the ring, however, the accelerometer was attached at the same location during every test. This produced a constant perturbation that did not effect test comparisons.

During the holographic tests, the aluminum ring was supported radially at each end by 8 elastic bands spaced at 45° intervals around the circumference. This configuration provided excellent stability while maintaining the free-free boundary condition employed during the impact hammer tests.

Figure 5 shows the panoramic holo-interferometry test setup used to obtain mode shape information from the aluminum ring. Two 38 mm (1.5") diameter PALs, with optical characteristics analogous to those contained in the imaging system shown in Figure 2, were spaced at a distance of 3.175 mm (0.125") apart and positioned with their optical axes aligned with the z-axis of the coordinate system as shown in Figure 3. The ring was positioned around the PALs with its longitudinal axis along z. The inner surface of the ring was painted white, and coherent light from a 400 milliwatt Argon-ion laser (λ = 514 nm) was projected onto the inner wall by expanding and collimating the object beam, and then passing the collimated beam through one of the PALs. An image of the ring was captured using a second PAL. A transfer lens was used to convey the virtual image, formed within the PAL itself, to a digitizing camera and computer system. As shown in Figure 5, a hologram of the wavefronts emerging from the second PAL was recorded using a thermoplastic holocamera positioned behind the transfer lens. It should be noted that the holocamera can also be positioned between the transfer lens and the PAL, or in the image plane. However, the latter condition causes excessive noise during

reconstruction, since anomalies such as dirt and pits in the thermoplastic are recorded along with the image of the cavity.

An HP 3562A Dynamic Signal Analyzer was used to perform sine sweep measurements on the ring once it was installed in the holographic setup. Response measurements were obtained with the aforementioned Piezotronics, Inc. accelerometer. Several attempts were made to utilize shaker excitation to drive the ring but the mass loading effects induced by the armature mass produced dynamic information that significantly differed from that obtained during impact hammer modal testing. Acoustic excitation, on the other hand, produced results that compared favorably with impact hammer modal testing and time average holograms were recorded with the ring resonating at the predetermined natural frequencies.

Standard modal holographic techniques were also employed to obtain holo-interferograms on one half of the outer surface of the ring. The boundary conditions and excitation methods used during these tests were identical to those employed when using panoramic holo-interferometry.

Results

Eighteen panoramic holo-interferograms of inplane flexural modes due to twisting and/or bending were acquired. Tables 1 and 2 list the corresponding resonant frequencies along with those obtained from the standard impact hammer modal tests.

The resonant frequencies obtained holographically are typically 1% lower than those acquired during the impact hammer modal tests. This frequency shift was attributed to a mass loading effect caused by painting the ring after impact modal tests were completed.

Figures 6 through 8 correspond to three separate mode shapes: an inplane flexural mode at 814.5 Hz due to bending & twisting, and two inplane flexural repeated roots at 3107.4 Hz and

3198.9 Hz due to bending. Each figure shows mode shapes that were acquired using (a) standard impact hammer modal testing, (b) standard holo-interferometry and (c) panoramic holo-interferometry.

TABLE 1: Inplane flexural modes due to bending
(semi-prismatic shape)

Mode Number	PAL Holography (Hz)	Impact Hammer (Hz)
1	354.1	357.8
1 (Repeated Root)	369.8	373.1
2	1005.6	1014.1
2 (Repeated Root)	1033.9	1045.3
3	1914.3	1931.2
3 (Repeated Root)	1988.7	2009.8
4	3107.4	3137.5
4 (Repeated Root)	3198.9	3232.0
5	4584.7	4635.0
5 (Repeated Root)	4664.9	4712.5
6	6297.8	6350.1
6 (Repeated Root)	6377.8	6450.6
7	8359.4	8450.0

TABLE 2: Inplane flexural modes due to bending and twisting (non-prismatic shape)

Mode Number	PAL Holography (Hz)	Impact Hammer (Hz)
1	814.5	823.2
2	2311.6	2333.2
2 (Repeated Root)	2460.9	2479.9
3	4019.1	4048.4
4	5775.3	5826.6

Discussion

Since the standard impact hammer tests produce information obtained from an accelerometer location relative to an excitation location, spatial definition is determined by the number of acquired points. The holographic patterns, on the other hand, maximize spatial definition by obtaining information for all points contained within the illuminated/viewed area.

As mentioned earlier in the paper, the extremely bright areas on the holograms correspond to nodes and the fringe patterns describe a topographical map of the displacement measured along the sensitivity vector. The standard holographic recordings were taken on the outside of the ring with a single illumination and observation point. The sensitivity vector was predominately along the line of sight and nearly constant across the field of view. The curvature of the surface, however, caused the sensitivity vector to vary significantly with respect to the surface normal. Since the displacement of the ring was predominately radial and along the surface normal, displacement is recorded with different sensitivities across the field of view. For example, along the horizontal diameter of the ring, the sensitivity vector is nearly aligned with the surface normal and displacement sensitivity is maximum. As the surface normal deviates from the line of sight, displacement is measured at reduced sensitivity. These variations make it difficult to quantitatively analyze the holo-interferograms.

The sensitivity vector for the panoramic holo-interferograms, on the other hand, is nearly radial across the entire field of view. At the edges of the illuminated band, $\mathbf{g}$ is inclined at $\pm 15^{\circ}$, introducing a $\pm 4\%$ variance in radial sensitivity. Since displacement is measured with nearly constant sensitivity, quantitative analysis is much less complex. In addition, the interferograms are recorded on the inner surface of the ring and over the entire area of interest.

The dotted line in Figure 6(a) corresponds to the undeformed ring, whereas the solid lines

depict the movement in the flexural mode. This animated display indicates that the ring oscillates about a circumferential line and that there are four nodal regions where the twist reverses. The nodal regions labeled as 1 and 2 are observed in the standard holo-interferogram but the interpretation of the pattern is difficult. The panoramic holo-interferogram, on the other hand, clearly shows the circumferential nodal line and all four of the transition regions.

In Figures 7 and 8, the oscillation of the ring is primarily radial; nodal lines appear at ten different locations over the circumference. The standard holo-interferograms reveal only four nodal locations. The shape of the fringes between nodes can be attributed to the slight twist in the section but the difference in the number of fringes between the nodes is caused by the variation in the sensitivity vector with respect to the motion. The impression is that the amplitude of the motion is significantly different between different nodes. The panoramic holo-interferograms, on the other hand, reveal all ten of the nodal locations; the number of fringes between nodes is approximately equal, giving the correct impression that the amplitude of vibration between nodes is approximately equal. This is illustrated by the figures corresponding to the standard impact hammer animated displays.

Any time one or more axes of symmetry exist in the mechanical system, repeated roots will exist.[7] Theoretically, the mode shapes shown in Figures 7 and 8 should have occurred at the same frequency; the nodes of one pattern should lie at the antinodes of the other. However, when the accelerometer's mass was collocated with an antinode, the repeated root's frequency dropped. No frequency shift occurred when the accelerometer was collocated with a node. Thus the accelerometer's mass separated respective repeated roots. This phenomenon occurred for all of the repeated roots observed during the investigation.

As compared to those in Figure 8, the fringe patterns in Figure 7 show that slight

perturbations occur in the inplane flexural modes due to bending. These semi-prismatic mode shapes occurred because the accelerometer was located at an antinode at the edge of the ring.

Conclusions

This paper expands on prior research performed in the area of panoramic holo-interferometry by developing an approach to qualitatively analyze time-average panoramic holo-interferometric fringes recorded within cylindrically shaped cavities. The approach has an advantage over modal hammer impact testing in that spatial definition is optimized. In contrast to standard time-average holo-interferometry, panoramic holo-interferometry allows a cylindrical region of the inner walls of a cavity to be viewed simultaneously, and radial displacements to be recorded with nearly constant sensitivity over the entire field of view. This unique capability facilitates qualitative analysis, since mode shapes can be readily visualized.

The research is expected to provide a new inspection/modal testing capability for the NASA's Space Shuttle Main Engine program, since many rocket engine components are cylindrically shaped. Future plans call for applying the technique to study bearing cages, high pressure turbo pump housings and turbine inlet bellows.

Acknowledgements

The authors would like to acknowledge the interest and support of Cliff Kirby and Danny Coleman of the Marshall Space Flight Center's Structures and Dynamics Laboratory for their interest and support of the research. Panoramic annular lenses were made available to the project by Optechnology, Inc., Gurley, Alabama.

References

1. Stetson, K.A., Powell, R.L., "Interferometric hologram evaluation and real time vibration analysis of diffuse objects," J. Opt. Soc. of Am., 55, (1965), pp. 1694-1695.

2. Mangin, F., French Patent No. 125.374; 1878.

3. Matthys, D.R., Gilbert, J.A., Greguss, P., "Optical measurements through panoramic measuring systems," Proc. of the SEM Conference on Hologram Interferometry and Speckle Metrology, Baltimore, MD, November 5-8, 1990, pp. 164-171. A short list of such patents is given in Reference 2 of that paper.

4. Gilbert, J.A., Greguss, P., Kransteuber, A.S., "Holo-interferometric patterns recorded through a panoramic annular lens," Proc. of SPIE's International UNESCO Seminar on 3-D Holography, Volume 1238, entitled 3-D Holography '89, Kiev, USSR, September 5-8, 1989.

5. Gilbert, J.A., Matthys, D.R., Hendren, C.M., "Displacement analysis of the interior walls of a pipe using panoramic holo-interferometry," Proc. of SPIE's 1991 International Symposium on Optical & Optoelectronic Applied Science & Engineering, San Diego, California, July 21-26, 1991, pp. 128-134.

6. Matthys, D.R., Gilbert, J.A., Puliparambil, J., "Panoramic holointerferometry," Proc. of the SEM Spring Conference on Experimental Mechanics, Dearborn, MI, June 7-9, 1993, pp. 920-929; to be published in Experimental Mechanics, 1995.

7. Allemang, R.J., Vibrations: Analytical and Experimental Modal Analysis, UC-SDRL-CN-20-263-662, 1990, p. 125.

List of Figures

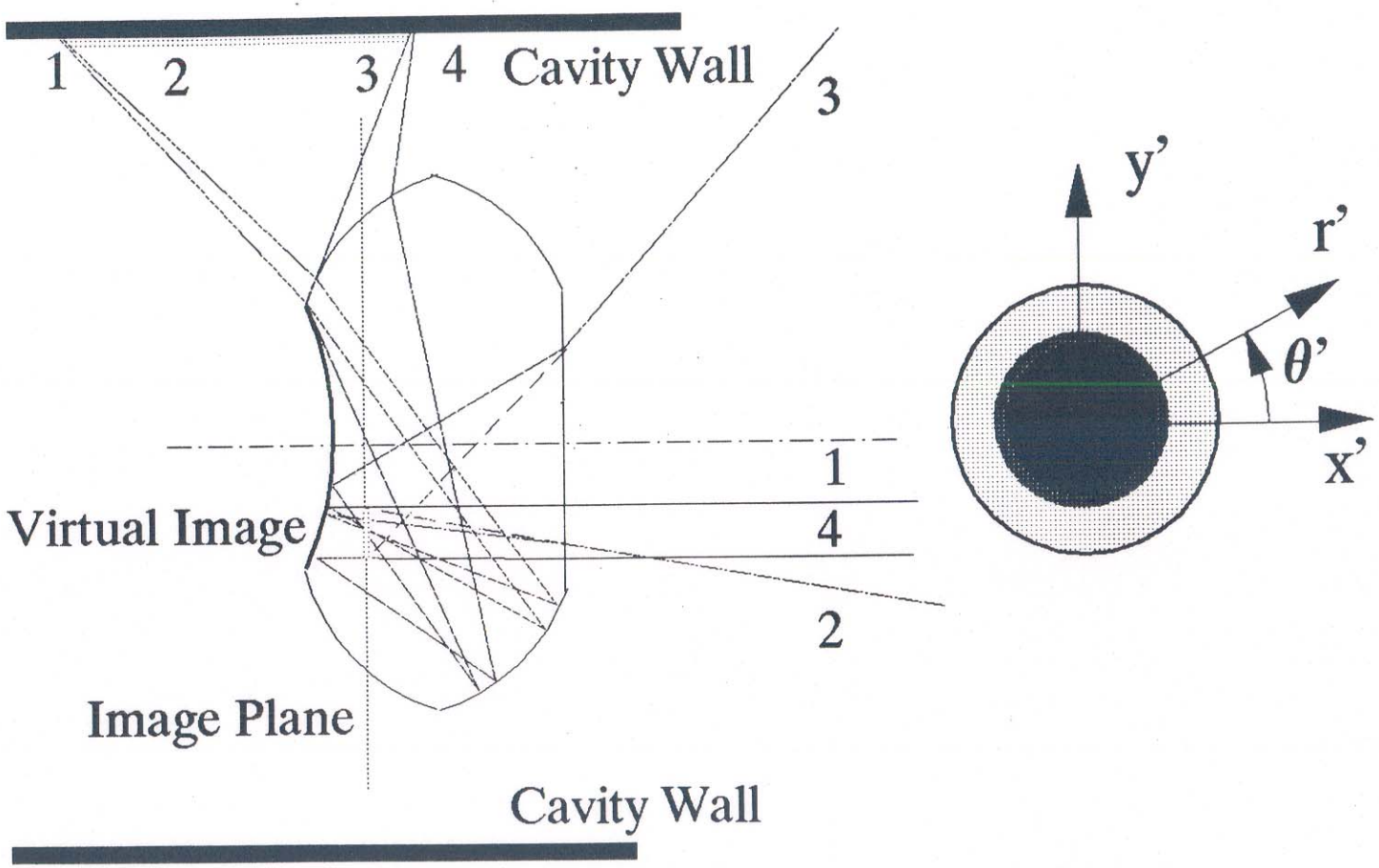

Figure 1. Ray diagram for a PAL; coordinate systems (x',y') and (r',θ') define the image plane.

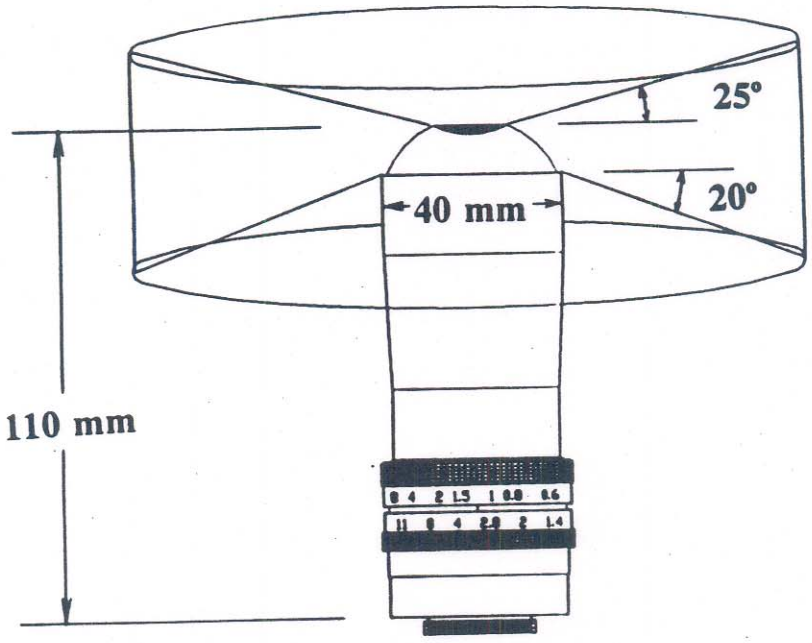

Figure 2. A 38 mm diameter PAL imaging system. Figure courtesy of Optechnology, Inc., Gurley, AL.

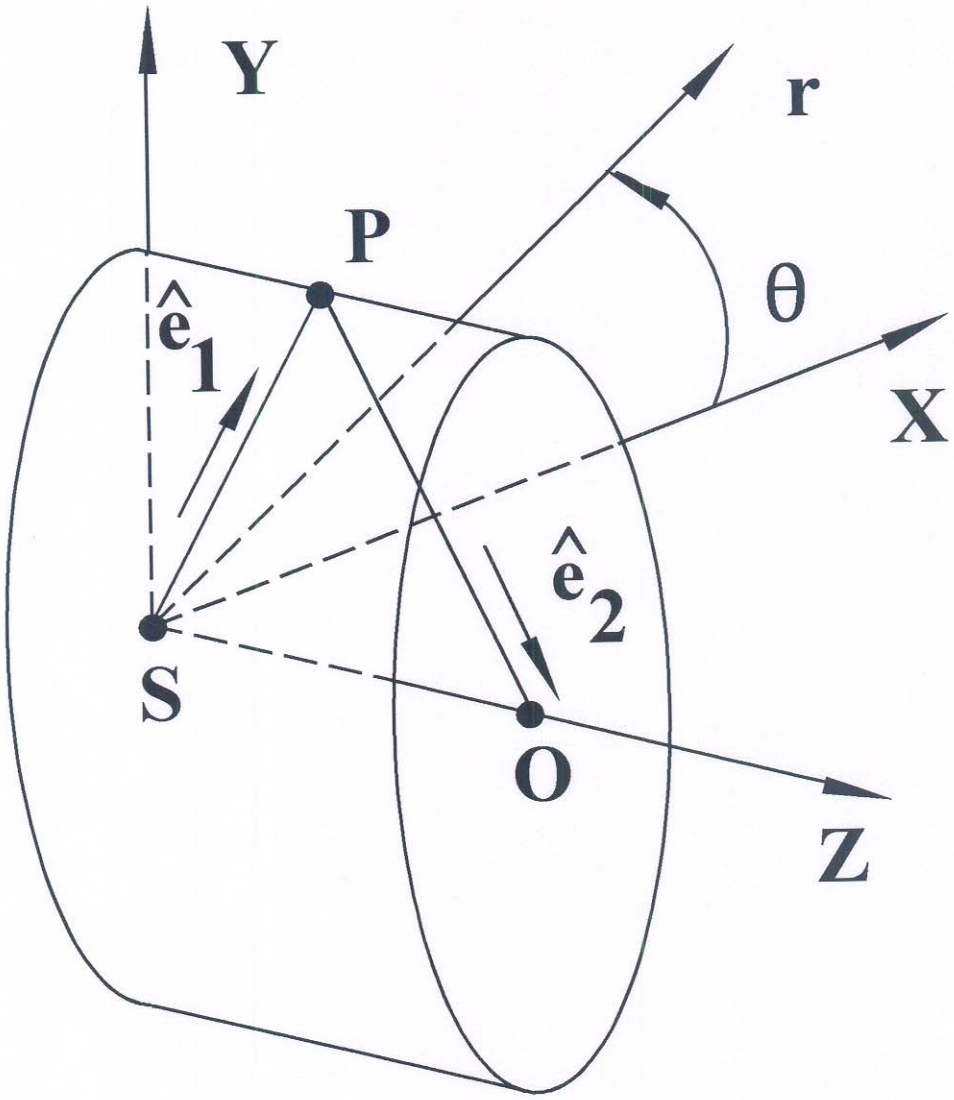

Figure 3. Cartesian (x,y,z) and cylindrical (r,θ,z) systems used to describe object space.

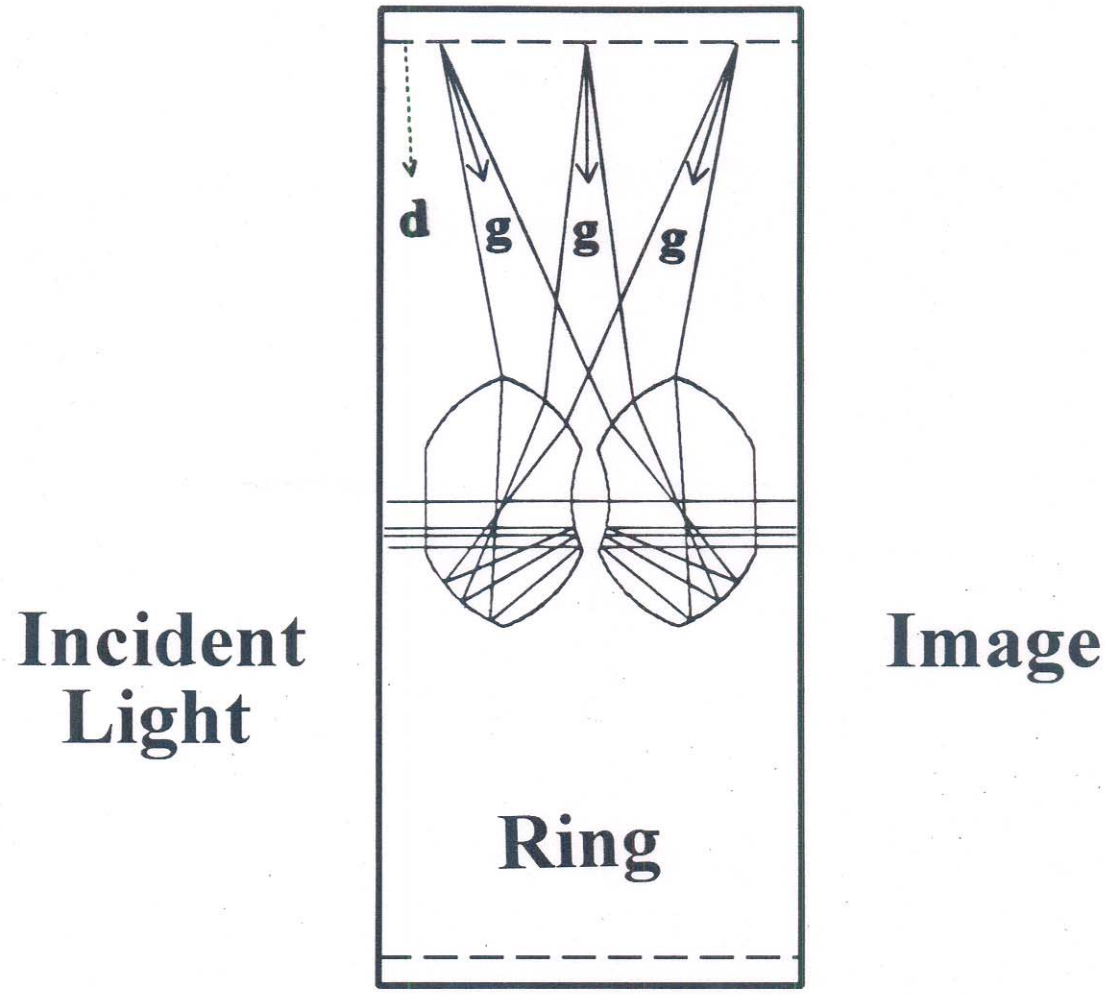

Figure 4. Figure to show the direction of the sensitivity vector.

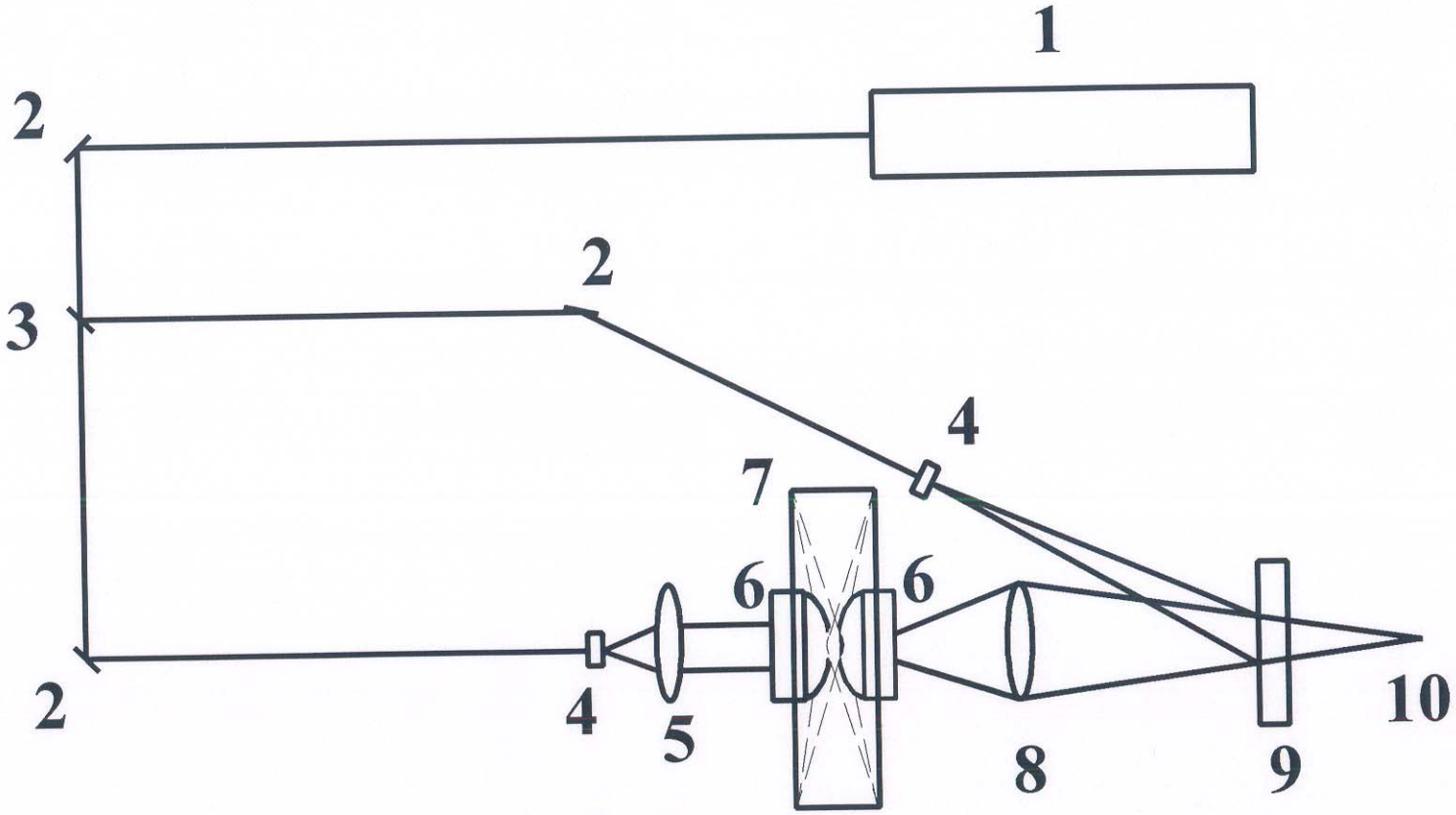

1. Laser
2. Mirror
3. Beam Splitter
4. Spatial Filter
5. Collimating Lens
6. PAL
7. Ring
8. Transfer Lens
9. Thermoplastic Plate
10. Image Plane

Figure 5. Experimental setup for recording panoramic holo-interferograms. A CCD camera is used to acquire images.

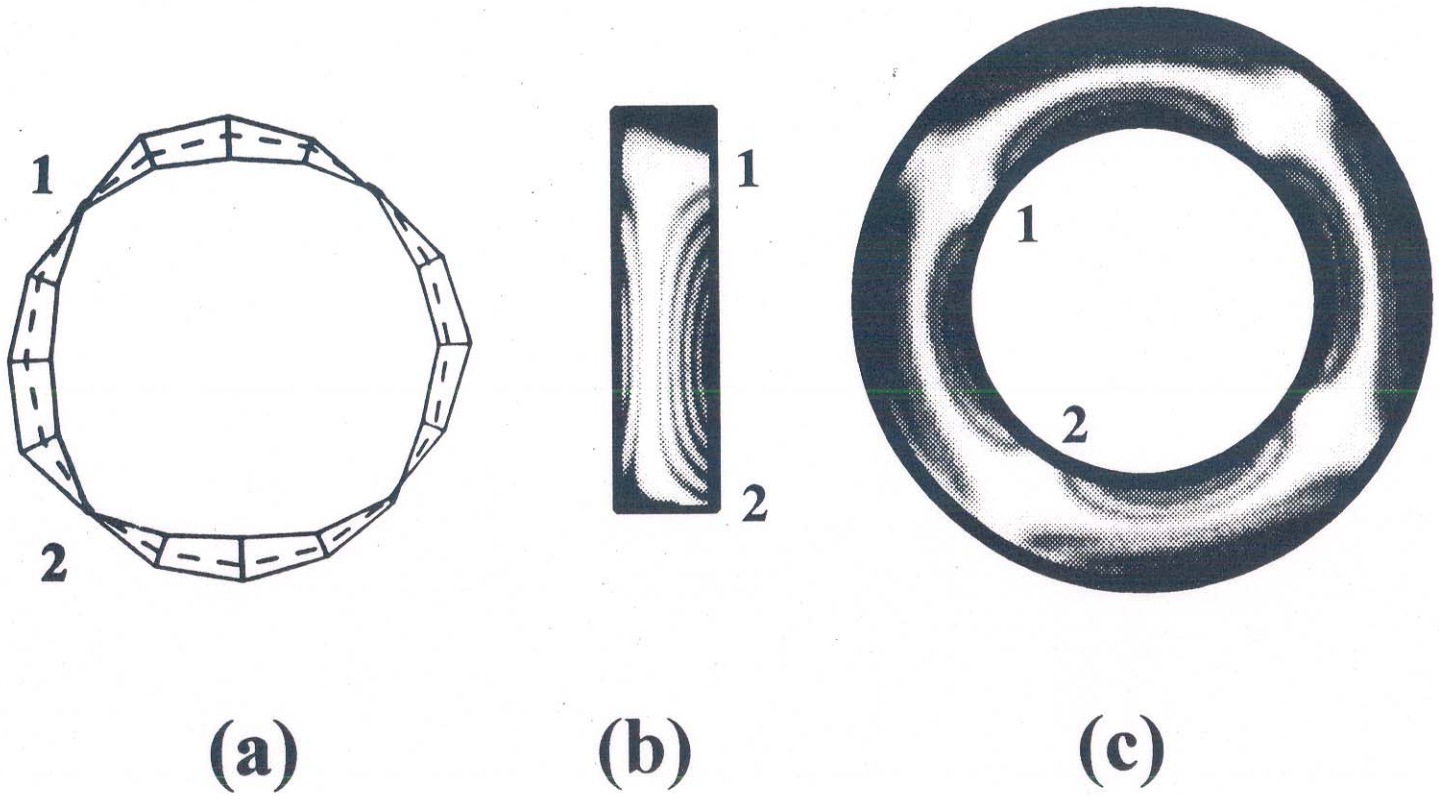

Figure 6. Results for an inplane flexural mode recorded at 814.5 Hz due to bending and twisting: (a) standard impact hammer animated display; (b) standard holo-inteferogram; (c) panoramic holo-interferogram.

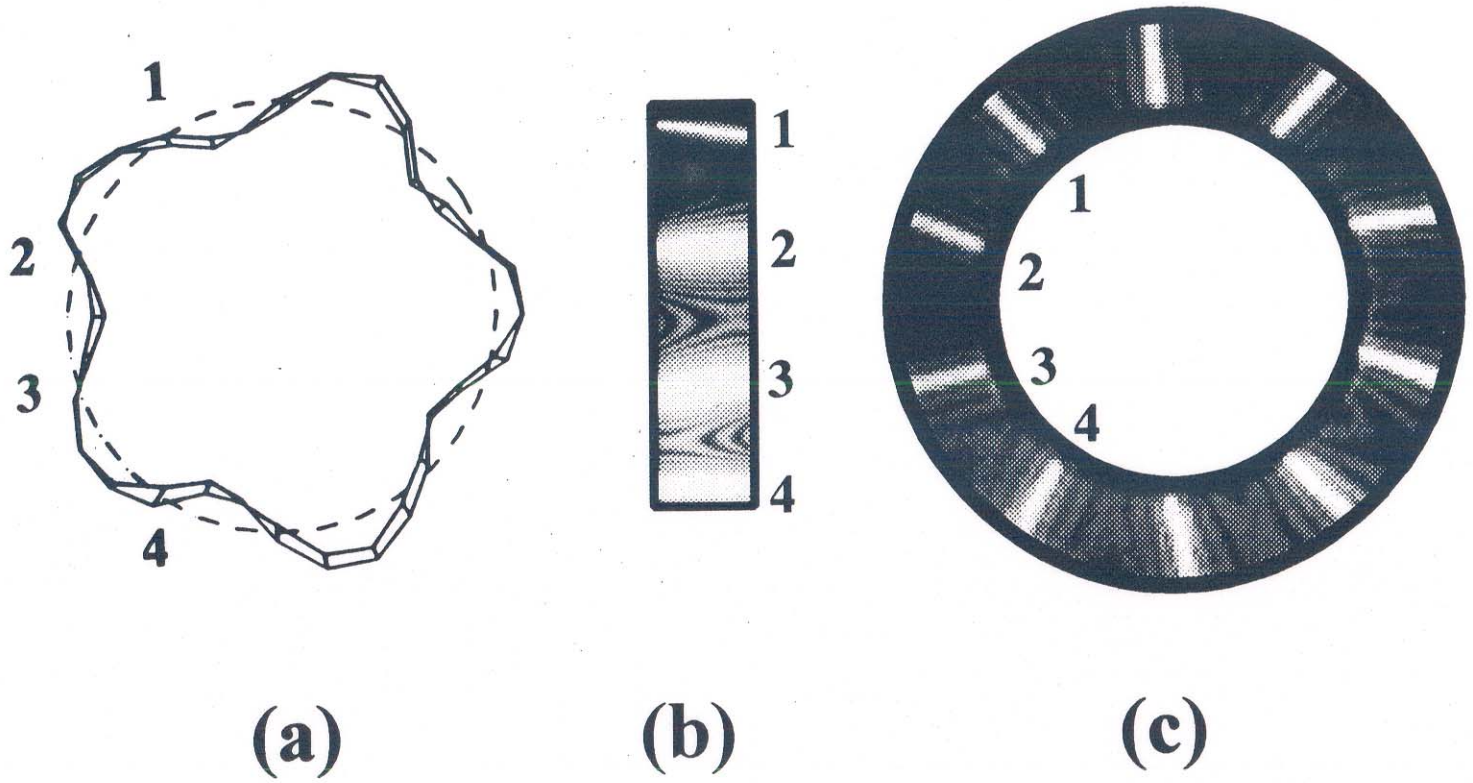

Figure 7. Results for an inplane flexural repeated root at 3107.4 Hz due to bending: (a) standard impact hammer animated display; (b) standard holo-interferogram; (c) panoramic holo-interferogram.

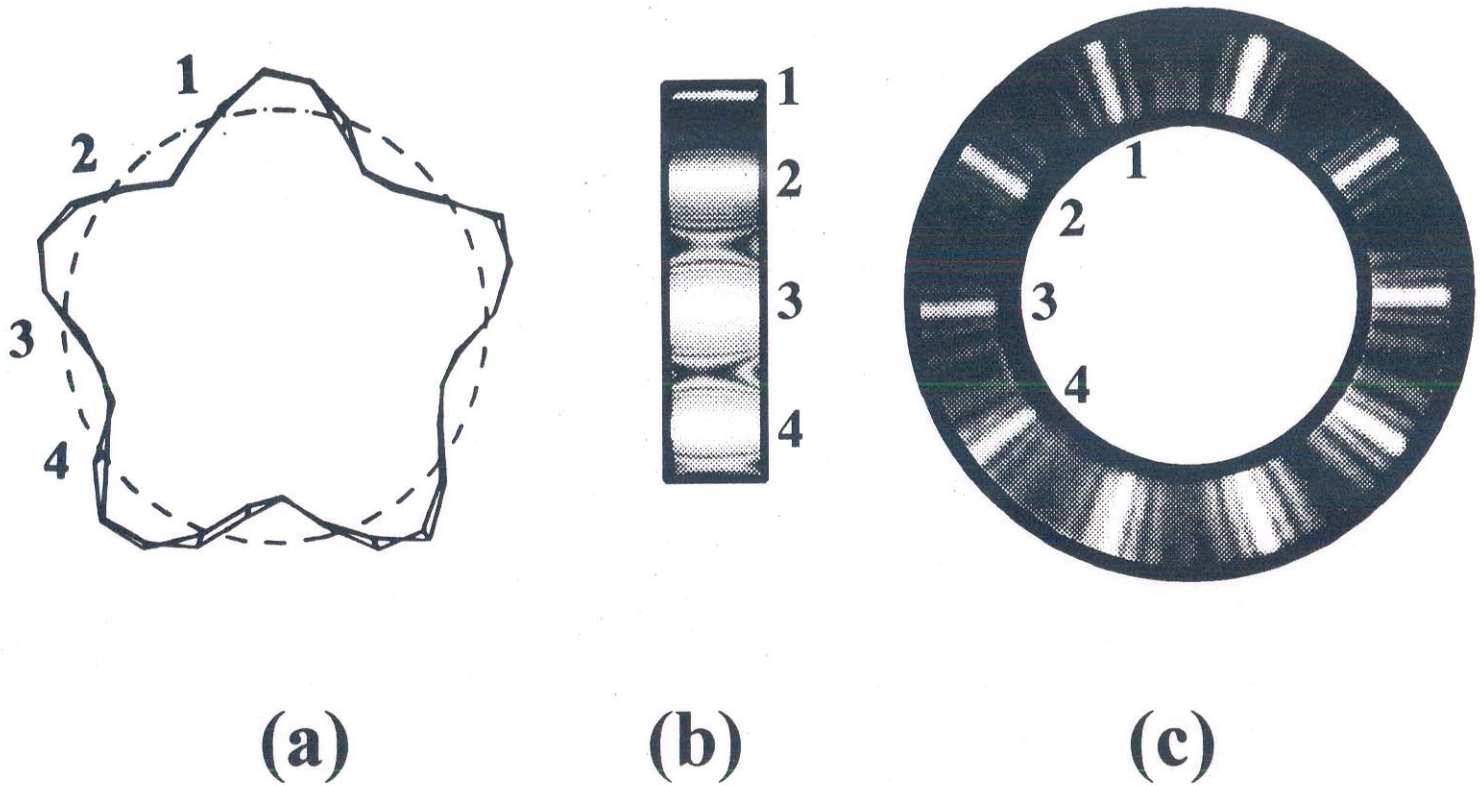

Figure 8. Results for an inplane flexural repeated root at 3198.9 Hz due to bending: (a) standard impact hammer animated display; (b) standard holo-interferogram; (c) panoramic holo-interferogram.